AIAA 92-3550

Vorticity Generation by Contoured Wall Injectors

I. A. Waitz

Massachusetts Institute of Technology
Cambridge, Massachusetts 02139

F. E. Marble and E. E. Zukoski

California Institute of Technology
Pasadena, California 91125

AIAA/SAE/ASME/ASEE
28th Joint Propulsion Conference and Exhibit
July 6-8, 1992 / Nashville, TN

VORTICITY GENERATION BY CONTOURED WALL INJECTORS

Ian A. Waitz*
Massachusetts Institute of Technology, Cambridge, Massachusetts 02139

Frank E. Marble† and Edward E. Zukoski‡
California Institute of Technology, Pasadena, California 91125

Abstract

A class of contoured wall fuel injectors was designed to enable shock-enhancement of hypervelocity mixing for supersonic combustion ramjet applications. Previous studies of these geometries left unresolved questions concerning the relative importance of various axial vorticity sources in mixing the injectant with the freestream. The present study is a numerical simulation of two generic fuel injectors which is aimed at elucidating the relative roles of axial vorticity sources including: baroclinic torque through shock-impingement, cross-stream shear, turning of boundary layer vorticity, shock curvature, and diffusive flux. Both the magnitude of the circulation, and the location of vorticity with respect to the mixing interface were considered. Baroclinic torque and cross-stream shear were found to be most important in convectively mixing the injectant with the freestream, with the former providing for deposition of vorticity directly on the fuel/air interface.

Nomenclature

c_{He}	helium mass fraction
h_i	height of injection plane
L	interface length
M	Mach number
p	static pressure
r	radius of curvature
U_∞	freestream velocity
V_S	shock propagation speed
x	streamwise, axial coordinate
$\bar{x}$	non-dimensional distance downstream of the injection plane, x/h_i
y	cross-stream coordinate
$\bar{y}$	non-dimensional cross stream coordinate, y/h_i
z	vertical coordinate
$\bar{z}$	non-dimensional vertical coordinate, z/h_i
α_c	compression angle of upper ramp surface
α_e	expansion angle of trough between injector ramps
β	shock wave angle
Γ	circulation
$\bar{\Gamma}$	non-dimensional circulation, $\Gamma/U_\infty h_i$
δ	boundary layer height
$\bar{\delta}$	non-dimensional boundary layer height, δ/h_i
ρ	density
$\vec{\omega}$	vorticity vector

* Assistant Professor of Aeronautics and Astronautics, Member AIAA

† Professor of Mechanical Engineering and Jet Propulsion, Emeritus, Fellow AIAA

‡ Professor of Mechanical Engineering and Jet Propulsion, Fellow AIAA

Introduction

This paper focuses on characterizing the axial vorticity generation mechanisms for a particular class of supersonic combustion ramjet (scramjet) fuel injection schemes. Investigations at lower speeds have shown that introduction of streamwise vorticity between two co-flowing streams can augment mixing by 30-100% beyond that associated with transverse shear (i.e. that driven by a velocity ratio between the two streams).[1] Geometries designed for introduction of streamwise vorticity have seen wide application in scramjet fuel injectors, combustor designs for reducing the oxides of nitrogen emitted from the proposed High Speed Civil Transport (HSCT), mixer/ejector designs to reduce noise from the HSCT, chemical lasers, and lobed mixers for mixing hot core flow with bypass air in current production turbofan engines.

The problem of providing loss-effective mixing in scramjets is particularly challenging. Flight speeds of Mach 15-20 dictate combustor flow speeds on the order of 5000 m/s. Further deceleration of the flowfield would produce an undesirable static temperature rise (limiting full energy release from the hydrogen-air reaction as a result of dissociation), and unacceptable total pressure losses. Thus for combustors of practical size, molecular-scale mixing must be achieved in less than one millisecond. This constraint, combined with weak compressible shear layer mixing, has driven extensive research into methods to enhance high-speed mixing.

Shock-Enhanced Mixing

The injectors that prompted this investigation were designed to enable shock-enhancement of hypervelocity mixing through employing baroclinic torque. While baroclinic torque was but one of several axial vorticity sources apparent in the geometries eventually tested, a short review of the fundamentals of shock-enhancement and baroclinic torque as they relate to mixing is appropriate, because of the important role it will be shown to play for these geometries.

Vorticity is created in a flow field at any point where a pressure gradient interacts with a non-parallel density gradient. This can be seen by considering the following source term in the vorticity equation,

$$\rho \frac{D}{Dt}\left(\frac{\vec{\omega}}{\rho}\right) = \frac{1}{\rho^2} \vec{\nabla}\rho \times \vec{\nabla}p$$

The dependence on the cross product dictates that the interaction must be between non-parallel gradients. This is possibly made clearer upon considering the diagrams shown in Figure 1 depicting the interaction of a non-uniform density fluid particle with a pressure gradient. Baroclinic torque is fundamentally a misalignment of the center of mass with the line of action of pressure forces on the particle such that a torque is produced. The necessary existence in scramjets both of pressure gradients associated with oblique shocks and fuel/air density gradients, spurred interest in baroclinic torque as a means for mixing enhancement through introduction of axial vorticity along mixing interfaces.

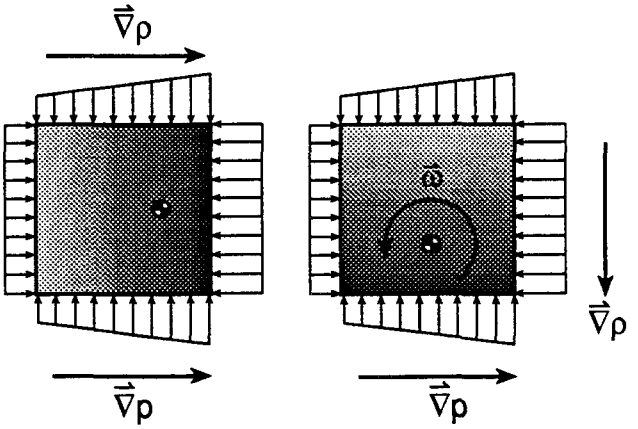

a. parallel gradients b. non-parallel gradients

Figure 1. Baroclinic torque

Several studies of the interaction of a shock with a density gradient have been performed. Their relevance to scramjet applications rests on the analogy depicted in Figure 2. The analytically and computationally more tractable two-dimensional, unsteady problem of shock passage over a light gas inhomogeneity is posed as a canonical model for the three-dimensional steady case of interest shown below it. While the analogy is limited by three-dimensional effects (and certainly unsteadiness in the real case), its usefulness as a qualitative, and to a limited extent, quantitative tool has been borne out by investigations of Marble, Hendricks, and Zukoski,[2] Yang,[3] and Drummond.[4] These works described the mixing associated with the convection of the density interface after deposition of vorticity as shown in Figure 2, and along with studies by Hass and Sturtevant,[5] prompted exploration of a low drag injection system in which the basic concept of shock-generated streamwise vorticity could be incorporated into a realistic scramjet injection scheme.

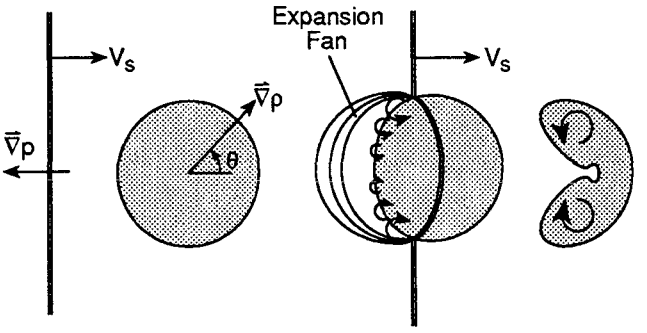

a. Two-dimensional, unsteady interaction of a shock with a light gas inhomogeneity.

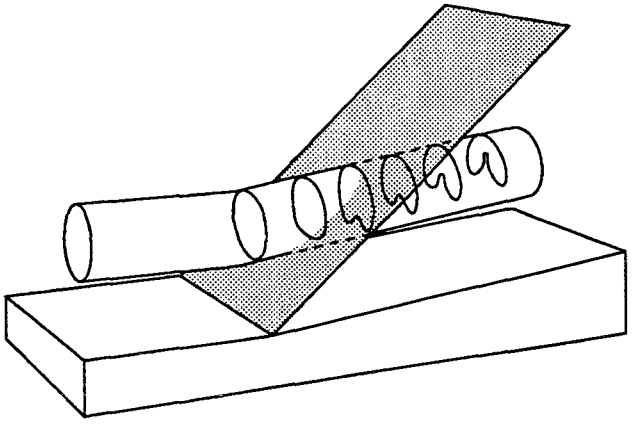

b. Three-dimensional, steady interaction of a column of light gas with an oblique shock.

Figure 2. Shock-enhanced mixing

Such a geometry was presented by Marble *et al.*[6] and is shown in the diagrams of Figure 3. It will be termed the 'baseline geometry'. The injector consists of alternate compression ramps and expansion troughs. The trough width is three times that of the ramp. The ramps are characterized by $\alpha_e = \alpha_c = 4.76^o$. Each ramp houses a two-dimensional nozzle discharging the injectant through

rectangular ports of aspect ratio 2. Fuel is injected parallel to the intended thrust vector to provide full use of the momentum of the injectant. In the plane of injection, the flow in the channels between the injectors is turned parallel to the freestream, forming a weak oblique shock. The design allows for the pressure gradient associated with this shock to intersect the density gradients existing between the light fuel and the air, generating axial vorticity via baroclinic torque, and providing strong convective mixing.

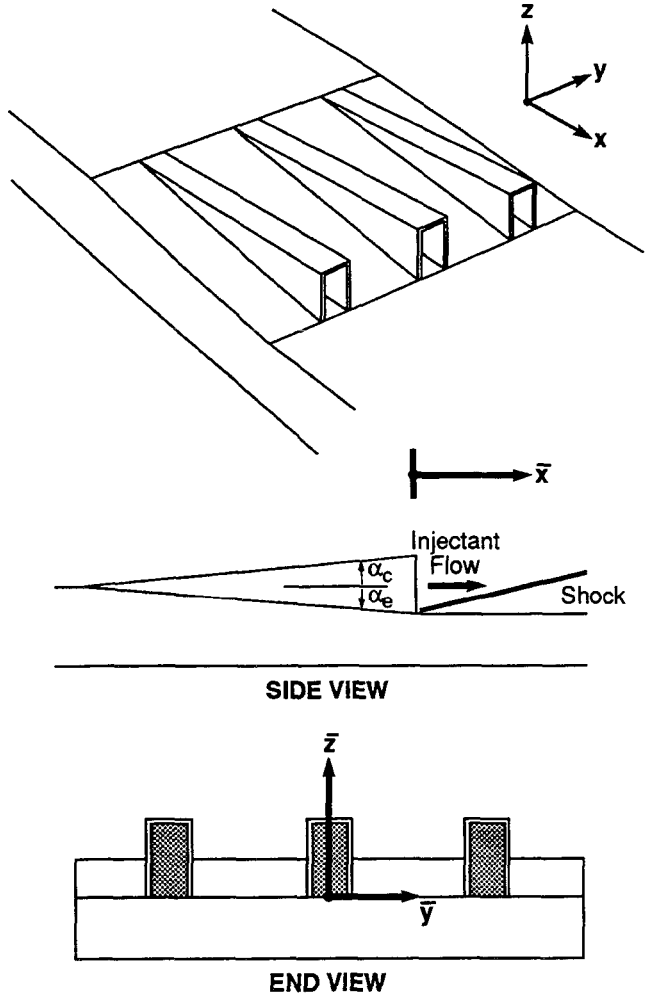

Figure 3. The baseline geometry

A broad study was undertaken to evaluate the performance of these injectors in terms of mixing, jet penetration, losses, and heating considerations.[7] This work included both experiments at the NASA Langley High Reynolds Number Mach 6 Wind Tunnel, and numerical simulations using a three-dimensional Navier-Stokes solver (SPARK3D). Helium was used as an injectant gas to simulate hydrogen fuel. A description of the flow phenomena associated with a single geometric configuration subject to fixed injectant and freestream conditions was presented by Waitz, Marble and Zukoski.[8] The effects of injector spacing, incoming boundary layer height, and injectant to freestream pressure and velocity ratio were addressed in a second publication.[9] One conclusion of these studies was that while the injectors were designed to enhance mixing through shock-impingement, other significant axial vorticity sources existed in the flow field as well. The complexity of the axial vorticity field downstream of these injectors is apparent in the plots of numerical data shown in Figure 4. (The plots were taken from reference 7. Barred quantities denote distances downstream of the injection plane normalized by the height of the injection plane, h_i. Vorticity of a negative sense is represented with broken lines.) The vortical flow rapidly lifted the injectant from the surface and provided strong convective mixing of the injectant/air interface. Within eight injector heights the vorticity coalesced into a counter-rotating vortex pair. Notably, the sense of the vortex pair was such that the induced velocities associated with it caused further migration of the injectant into the freestream. The complexity of the flow field, however, makes interpretation of the relative roles of the different axial vorticity sources difficult. This motivated the current investigation.

Scope of the Investigation

The aim of this work was to characterize the relative effectiveness of axial vorticity sources in terms of their influence on mixing the injectant with the freestream. While specialized to the injector shown in Figure 3, the results of this paper may be extended to a broader class of contoured wall injectors including those considered in some detail by personnel at NASA Langley Research Center and elsewhere.[10-17]

Conclusions will be drawn primarily from numerical simulations. Support for the validity of these simulations in representing the time-mean flow field centers on the agreement found between previous simulations and experimental flow field surveys.[7-9] In particular, quantitative agreement (on the order of better than ± 20%) was found with respect to large-scale kinematical behavior (Here 'large-scale' denotes flow phenomena of > 1/5 h_i, where h_i is the height of the injection plane.), static pressure signatures, and boundary layer behavior. Only qualitative agreement between mixing rates was displayed because of the limited scope of the code with respect to turbulence modeling. This is discussed in more detail below. Given a basis to support the simulations as representative of some important aspects of flow field behavior, heuristic extensions of the experimental test matrix were conducted numerically. The results of these investigations are the subject of this paper.

Numerical Method

The numerical simulations of the flow about the contoured wall injectors were performed using the SPARK3D program developed at NASA Langley Research Center.[10,11] The code integrates the Reynolds-averaged Navier-Stokes

equations for a multiple species system undergoing finite-rate chemical reaction. The code has been used by many investigators to model both reacting and non-reacting flow about scramjet injection geometries.[12-17] For all of the studies discussed herein, a non-reacting system in which Mach 1.7 helium was injected into a Mach 6 air freestream was modeled as it corresponded to previous experimental tests. The difficulties in accurately modeling the time mean of turbulent mixing without significant tuning were avoided by a preemptive decision to limit the scope of the simulations to a laminar model. Thus, comparison of mixing rates with the experimental data were only allowed on a qualitative basis. Direct quantitative comparison between numerical cases was allowed within the scope of the modeling.

The simulations were conducted on a domain extending one-half injector wavelength. (The data presented are mirrored about the symmetry plane.) Symmetry conditions were used to simulate an infinite array of injectors in the y-direction. No-reflection boundary conditions were used on the top of the domain simulating a semi-infinite freestream. Either free-slip or viscous conditions were applied on the combustor surfaces as required. For the viscous cases, a fully-developed turbulent boundary layer profile of specified thickness was modeled at the inlet to the computational domain. (Note that its growth from that point on was driven by laminar mechanics.) For all of the cases presented the helium was injected parallel to the downstream combustor wall, with velocity and pressure matched to that of the farfield. For additional details of the manner in which the code was used, the reader is referred to reference 7.

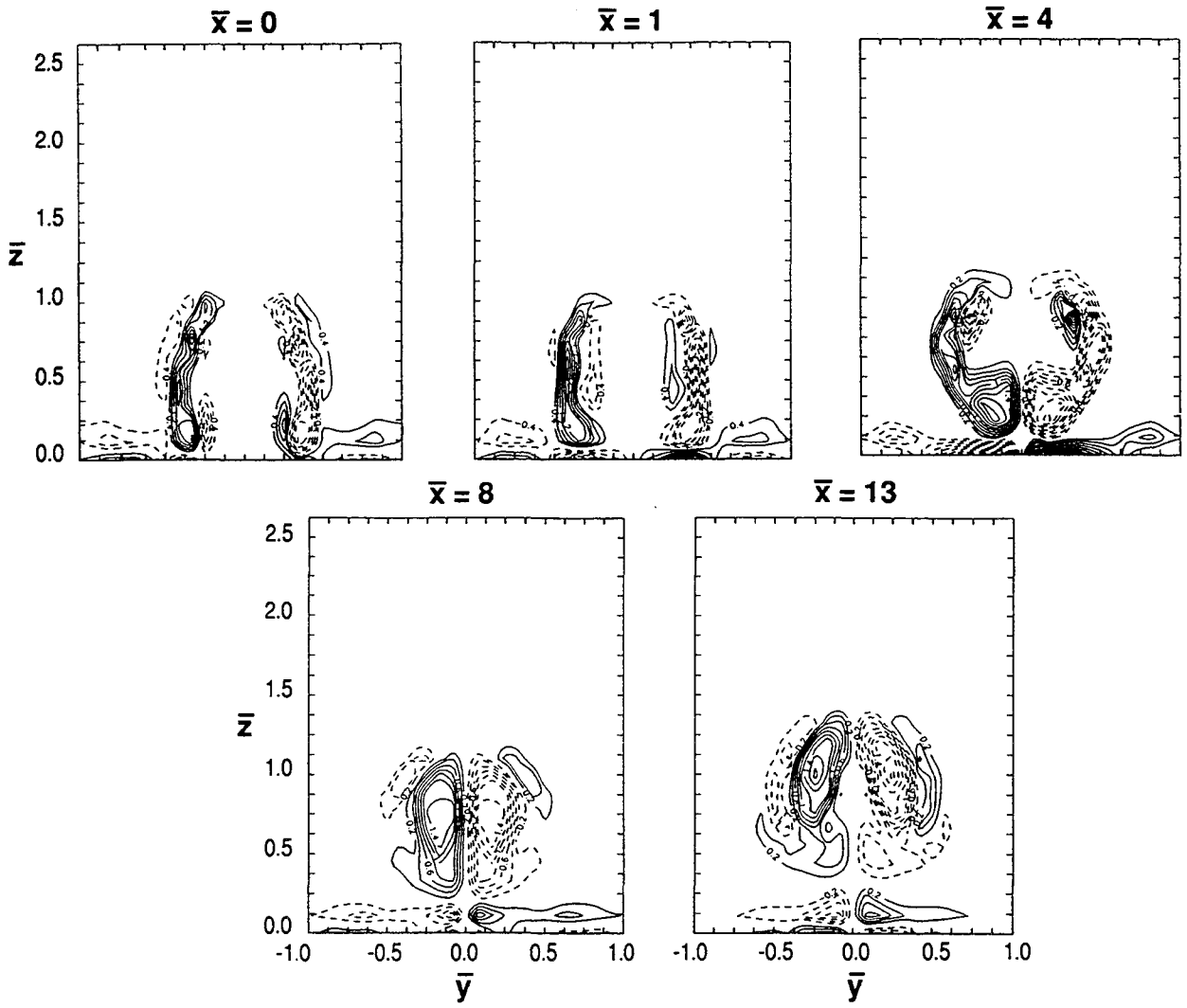

Figure 4. Contours of axial vorticity, ω_x (h_j/U_∞), baseline geometry, $\bar{\delta} = 0.2$, M = 1.7 helium injection, pressure and velocity matched to M = 6 air freestream.

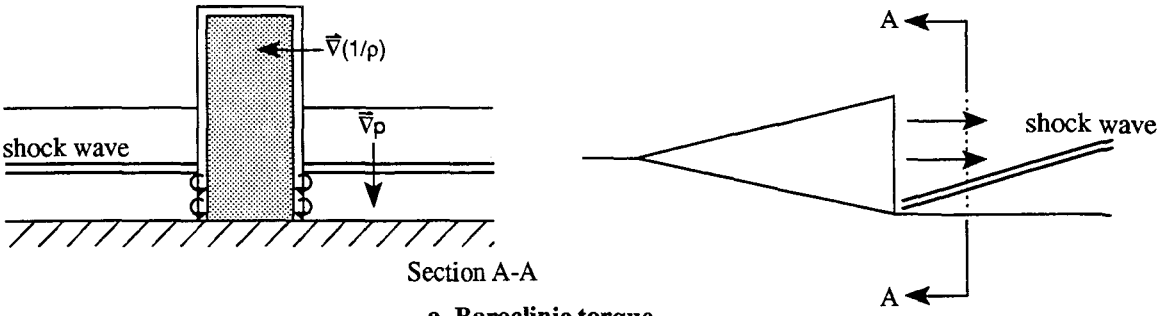

a. Baroclinic torque

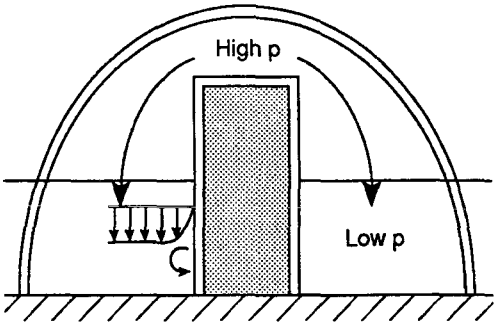

b. Cross-stream shear

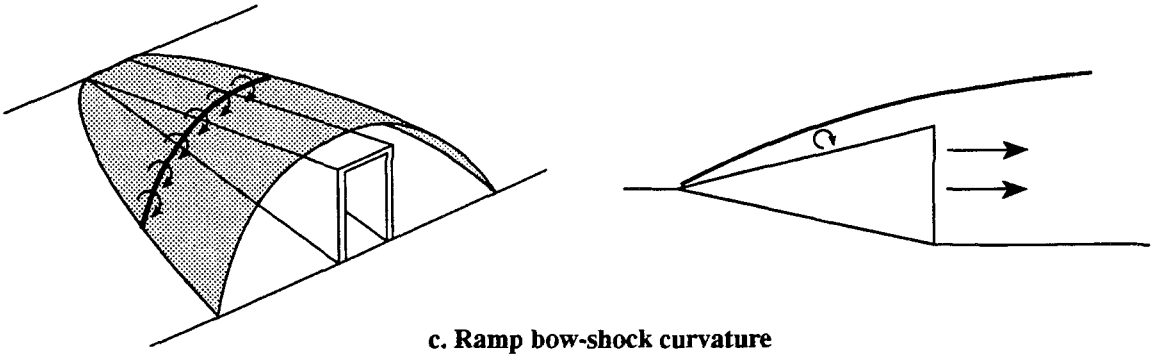

c. Ramp bow-shock curvature

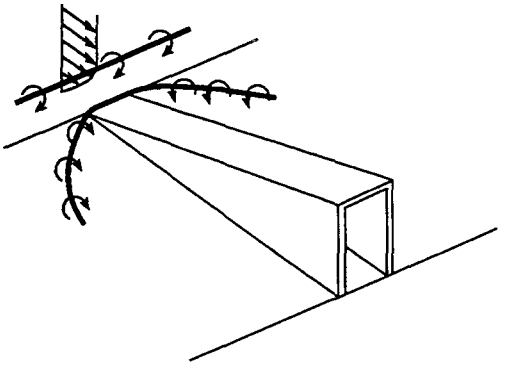

d. Turning of upstream boundary layer vorticity

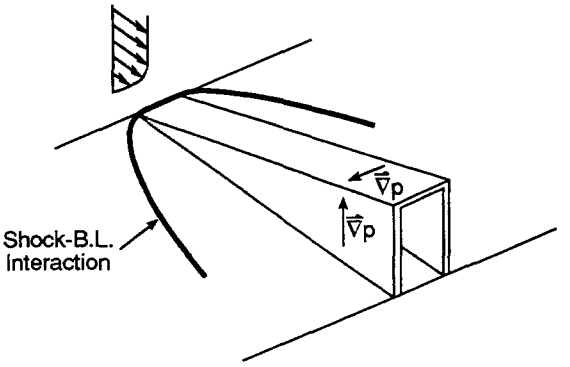

e. Diffusive flux of vorticity

Figure 5. Vorticity sources for contoured wall injectors.

Vorticity Sources/Modifiers and Geometries Investigated

Prior to presenting the results of the numerical simulations, a general discussion of vorticity sources and modifiers is necessary. Though the interest is in streamwise vorticity, the discussion will be limited primarily to axial vorticity as it is most convenient to evaluate numerically, and for these flows is typically within 5^o to 10^o of the streamwise direction. It should be noted that the action of the streamwise vorticity is two-fold: 1) it is associated with shear flow mixing at the interface - e.g. Kelvin-Helmholtz type instability and 2) it convects and stretches the mixing interface, increasing interfacial surface area. Only the latter of these was sufficiently resolved numerically. Further, streamwise vorticity is but one component of the mixing equation. Transverse shear (or that normal to the streamwise vorticity) is also very important, particularly as it often provides mixing on a much different scale than associated with convection from streamwise vorticity. The importance of the existence of a variety of scales has not been broached for flows in this speed and compressibility regime. Work at lower speeds by McCormick[18] has shown that these interactions may be important.

Various steady sources for axial vorticity in contoured wall injectors include a) baroclinic torque through shock interaction with the density interface, b) cross-stream shear in the exit plane of the nozzle driven by pressure gradients about the ramp, c) ramp bow-shock curvature, d) turning of the incoming boundary layer, and e) diffusive flux from the walls in the ramp region, particularly that driven by strong pressure gradients including shock-boundary layer interaction. These sources are displayed pictorially in Figure 5 with letters corresponding to the letters above. Note that sources d) and e) impact the level of cross-stream shear if they occur on the walls of the injector ramps. Given these sources/sinks for vorticity, in general the magnitude of the component in the axial direction downstream of the ramps is affected by turning, stretching, additional production, and diffusion. Simple models and analysis of the sources listed above were used to estimate their impact on levels of axial vorticity associated with the geometries and parameter ranges investigated.

The goal of the effort was to perform a rough quantitative grading of these vorticity sources and, more particularly, to detail their relative impact on large-scale convective mixing. The geometry of direct interest was the baseline geometry shown in Figure 3. To more clearly separate the influences of these axial vorticity sources, numerical modeling of two generic geometries was performed. The first of these is shown in Figure 6 and will be called the 'shock-enhancement' geometry. The geometry provides shock-generated vorticity as the uniform flow around the injectant is compressed in the exit plane. The geometry was designed with $\alpha_e = 4.76^o$ to produce baroclinic torque of roughly the same magnitude as that generated by the baseline model. Cross-stream shear is also important for this geometry, and is easily calculated for the uniform flow upstream of the injection point, being related geometrically to the angle of inclination of the ramp. The second geometry, shown in Figure 7 and called the 'no shock' geometry, produced no shock-generated vorticity, but strong cross-stream shear due to pressure gradients about the ramp. With $\alpha_c = 9.46^o$ this geometry was designed to produce levels of cross-stream shear similar to the baseline geometry (which had nearly the same included angle, $\alpha_c = 4.76^o$, $\alpha_e = 4.76^o$). Other axial vorticity sources were also present for this case much as they were for the baseline geometry. Often these were remote from the mixing interface like shock curvature and generalized boundary layer effects, including turning, diffusion and shock interaction. The ability to numerically simulate a free-slip boundary condition was useful in removing the flow complexities associated with the boundary layer.

Numerical Results

Numerical simulations were conducted for the shock-enhancement geometry and the no-shock geometry for boundary layer conditions of $\bar{\delta} = 0.0$ (free-slip), 0.2 and 1.0, where $\bar{\delta} = \delta/h_i$. Helium mass fraction contours at various planes downstream of the injection point are shown for the two geometries in Figures 8 and 9. The cases shown are for a finite thickness boundary layer, $\bar{\delta} = 0.2$. As with the baseline geometry, the streamwise vorticity associated with both geometries convectively mixed the injectant, coalescing into a counter-rotating vortex pair of a sense that produced migration of the injectant into the freestream. For both injectors, increasing the boundary layer scale adversely affected the large-scale convection of the jet. One difference between the two geometries was the amount of injectant left at or near the wall. Complete, rapid lift-off of the jet occurred for the case of baroclinic vorticity generation. Similar behavior was seen for the baseline geometry of Figure 3. This was a result of the location at which vorticity was formed with respect to the location of the helium jet.

This result is more clearly understood by considering in detail the generation of vorticity in each of the two test geometries. For clarity the following discussion is directed towards the numerical cases simulating an inviscid boundary condition. Figure 10 contains static pressure contours for several computational planes for the shock-enhancement geometry. The intersection of the shock with the density gradient between the injectant and the air is apparent. Streamwise vorticity was deposited along this intersection. The final plane shown displays a pressure signature characteristic of the counter-rotating vortex pair that was formed after the vorticity coalesced. The vorticity field for this case is shown in Figure 12. Vorticity of a negative sense is marked with broken lines. As the injectant passed through the oblique shocks, vorticity was deposited on the

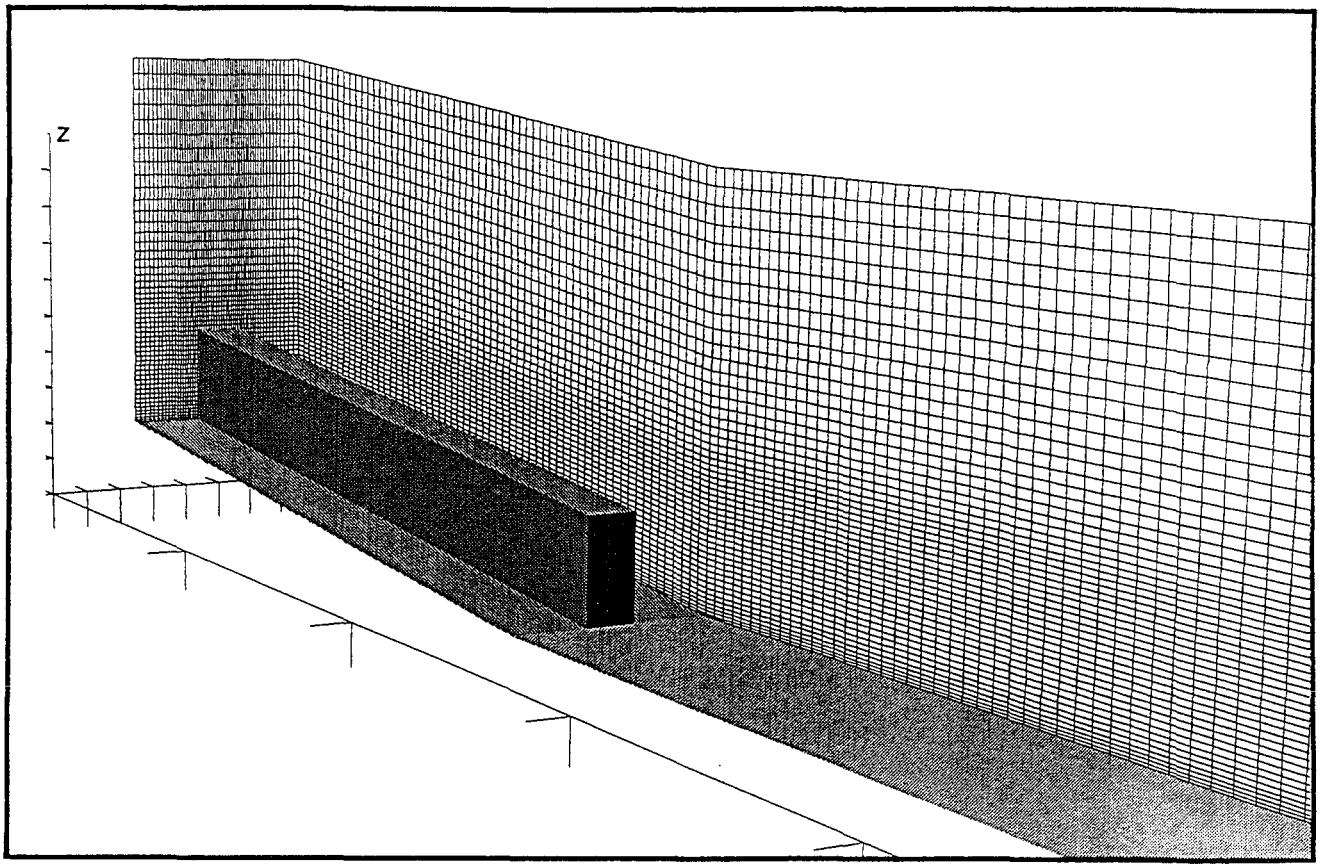

Figure 6. The shock-enhancement geometry.

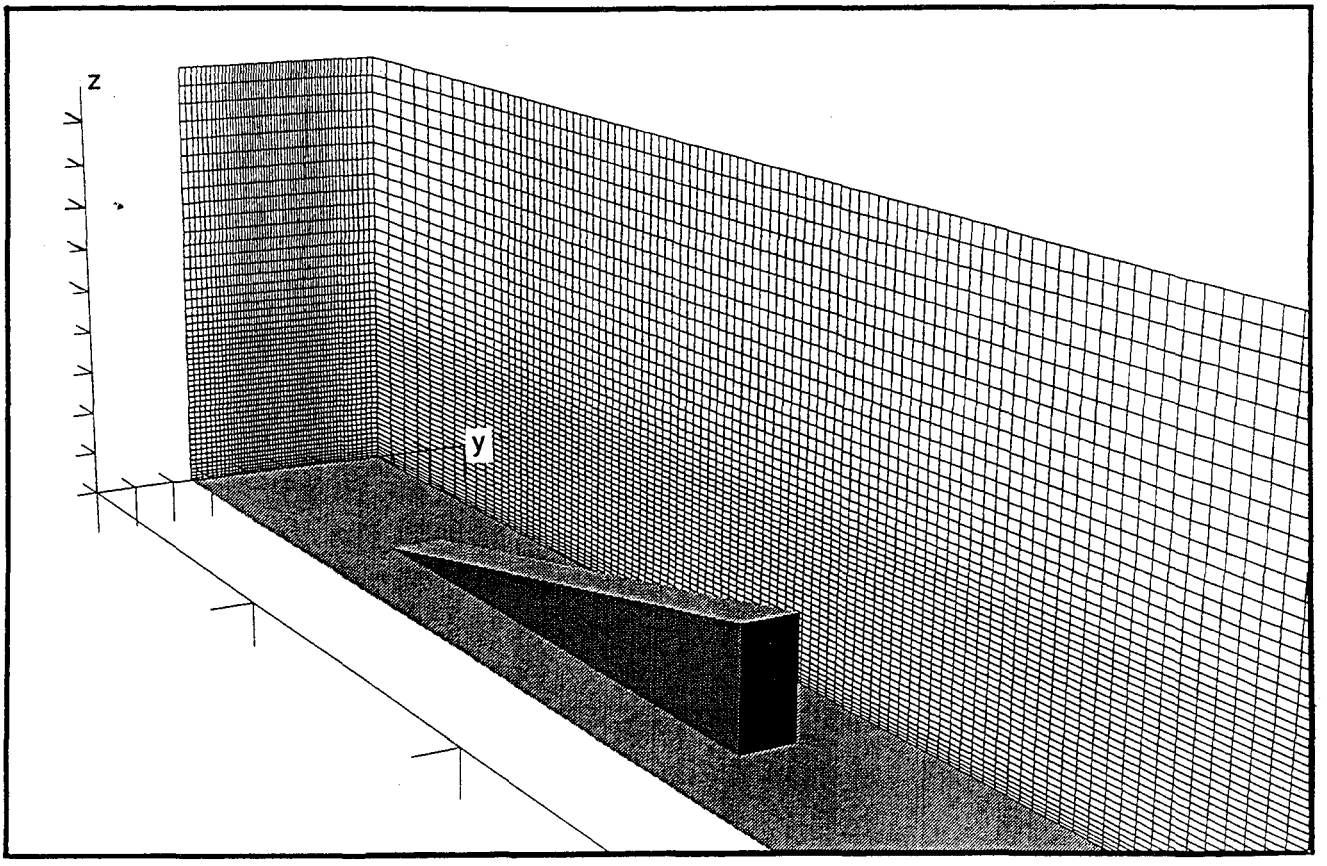

Figure 7. The no-shock geometry.

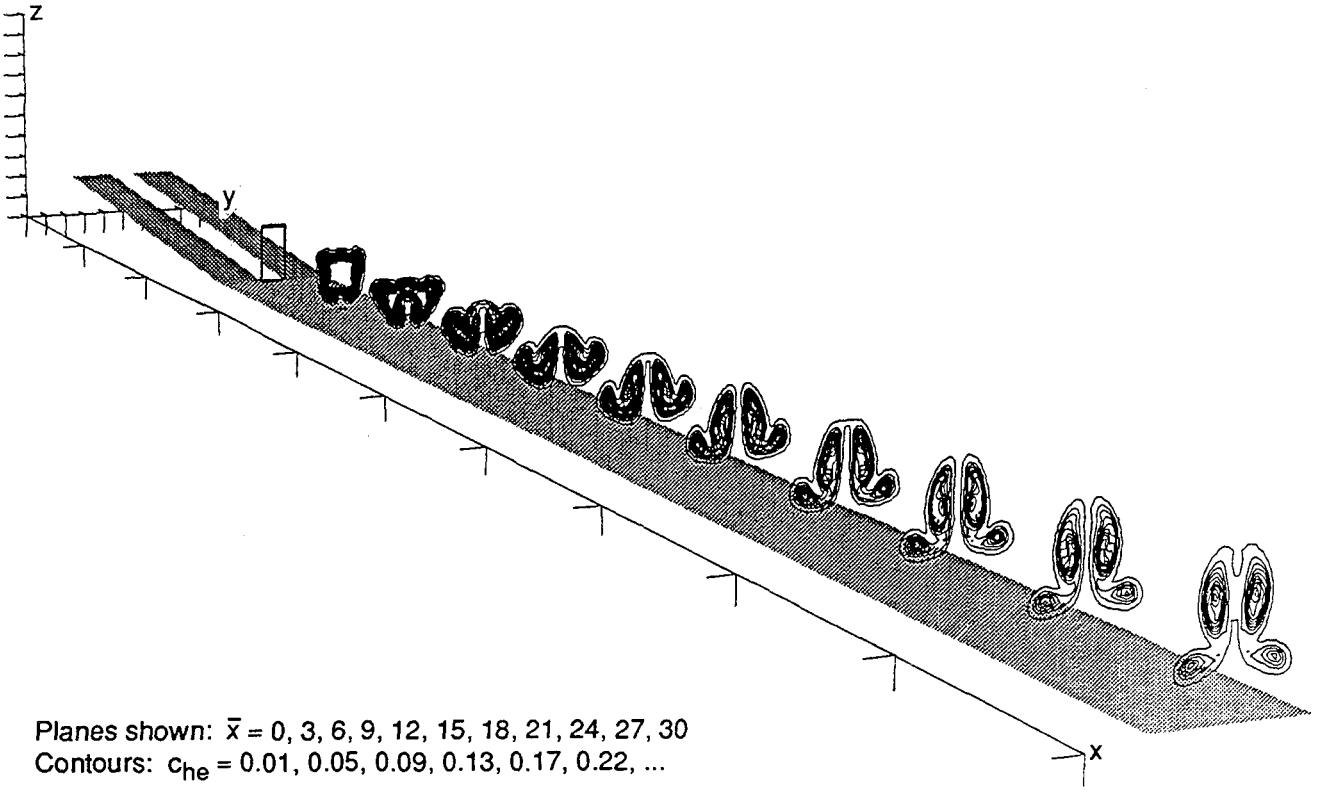

Figure 8. Contours of constant helium mass fraction. The shock-enhancement geometry, $\bar{\delta} = 0.2$.

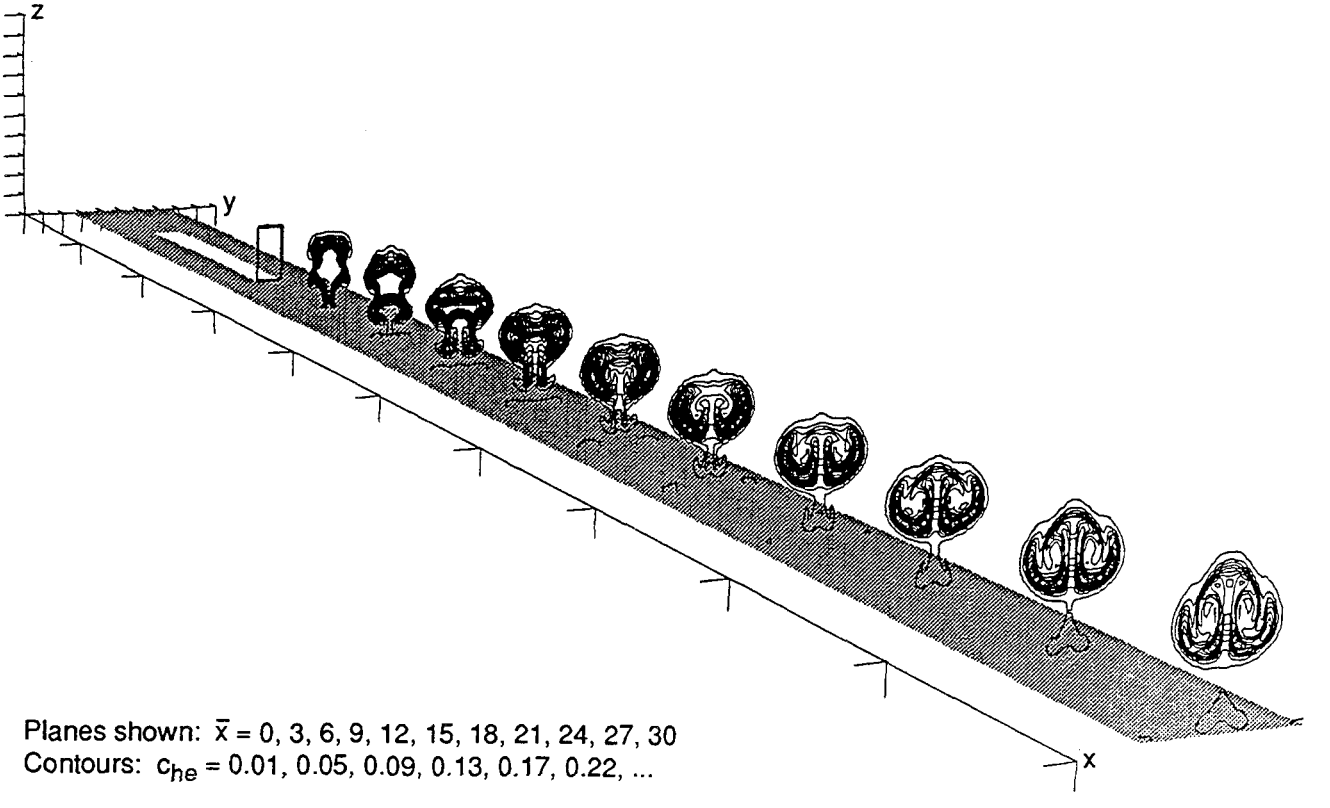

Figure 9. Contours of constant helium mass fraction. The no-shock geometry, $\bar{\delta} = 0.2$.

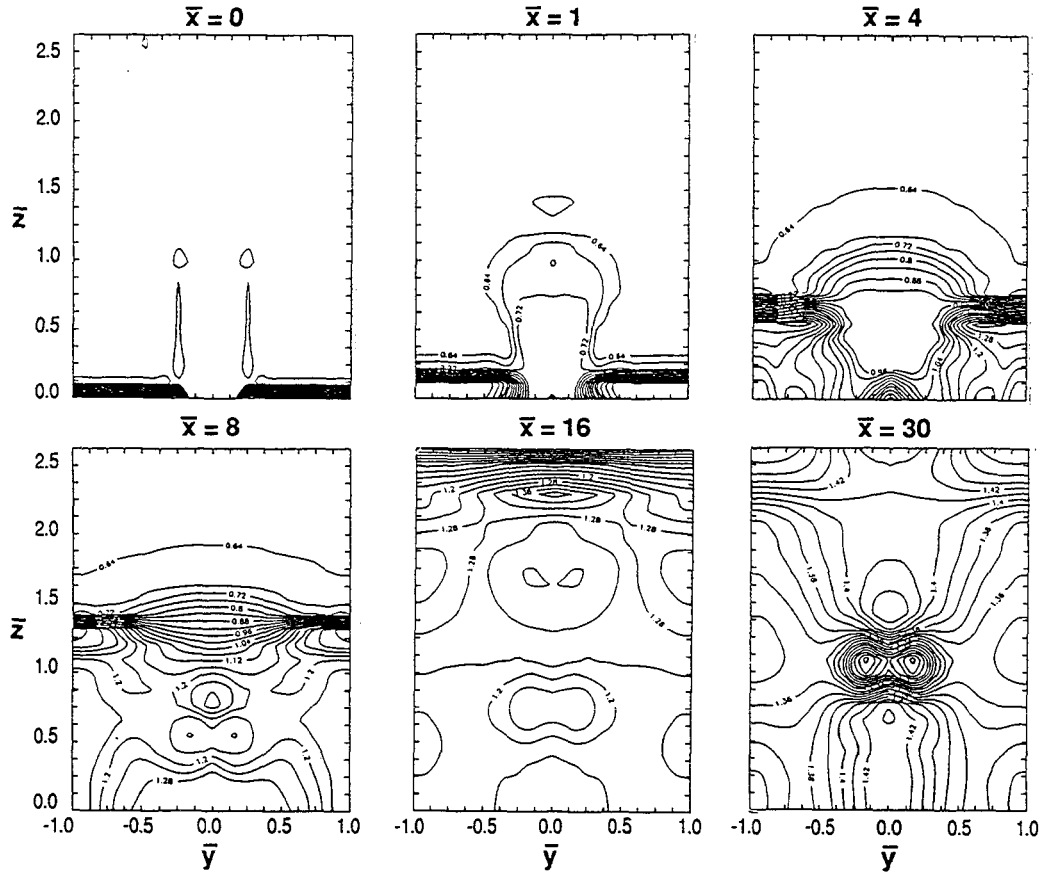

Figure 10. Static pressure signatures (psia). The shock-enhancement geometry, inviscid boundary conditions.

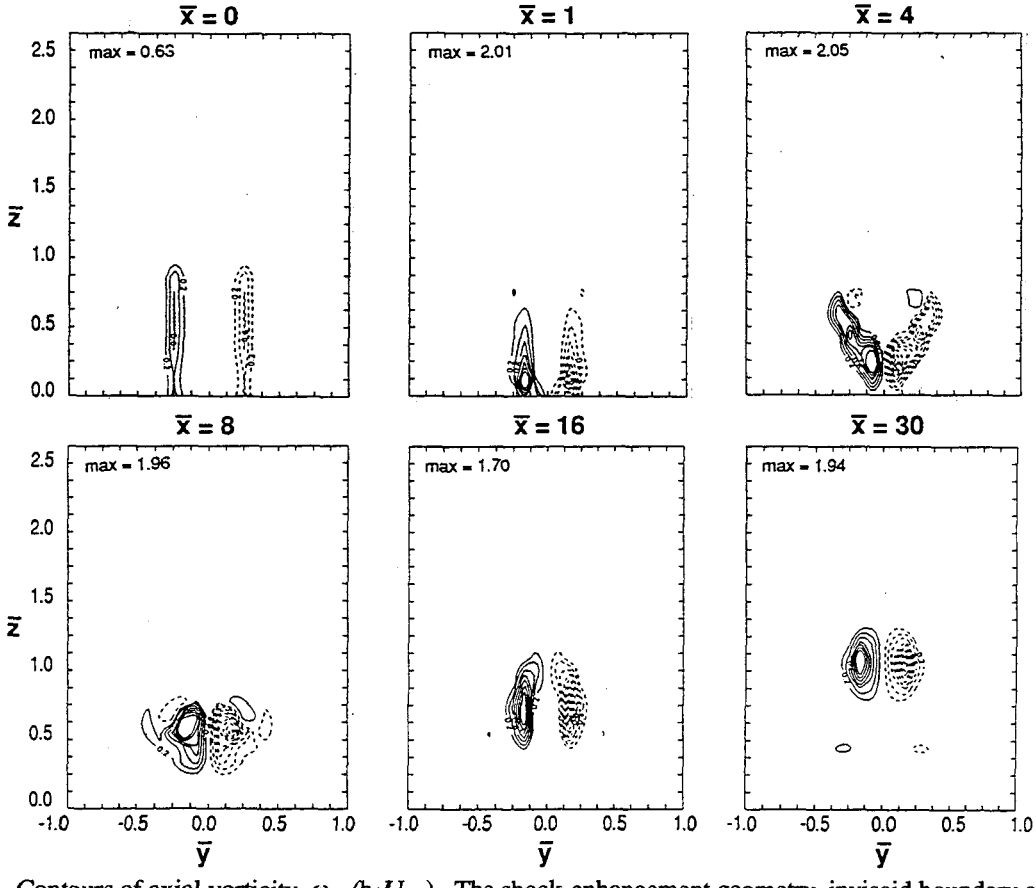

Figure 11. Contours of axial vorticity, $\omega_{\bar{x}}$ (h_i/U_∞). The shock-enhancement geometry, inviscid boundary conditions.

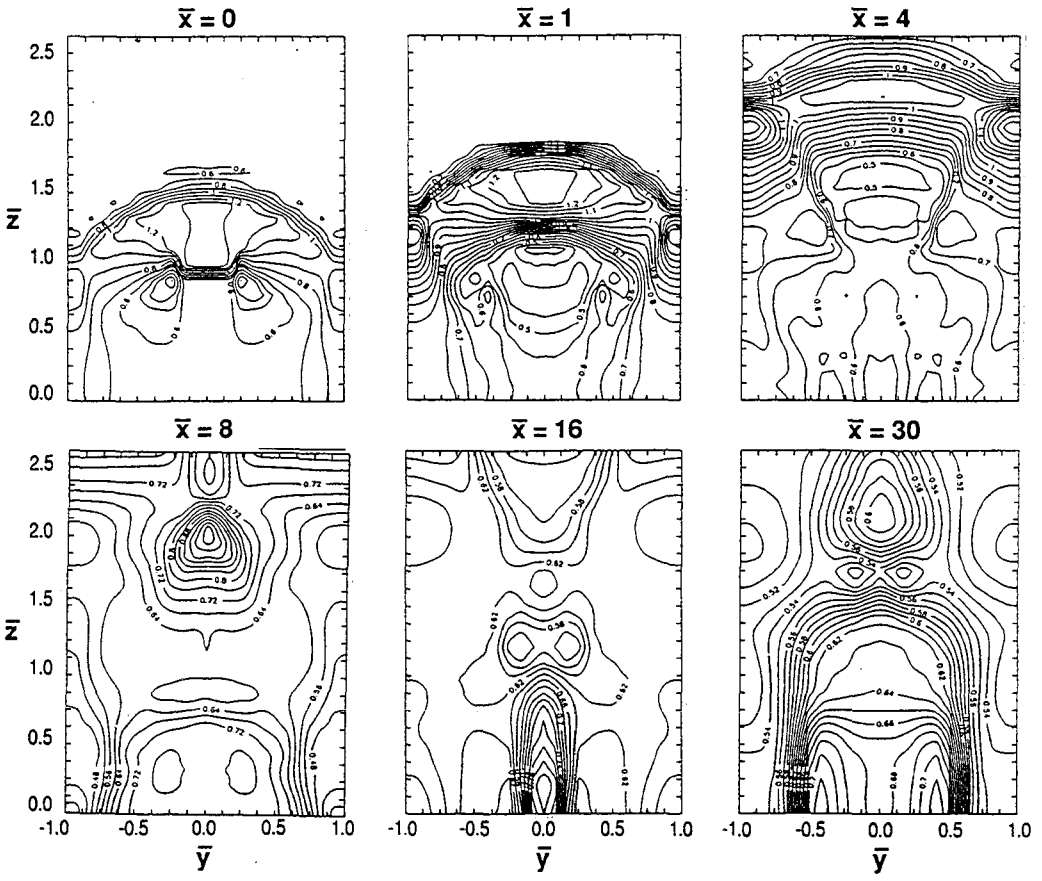

Figure 12. Static pressure signatures (psia). The no-shock geometry, inviscid boundary conditions.

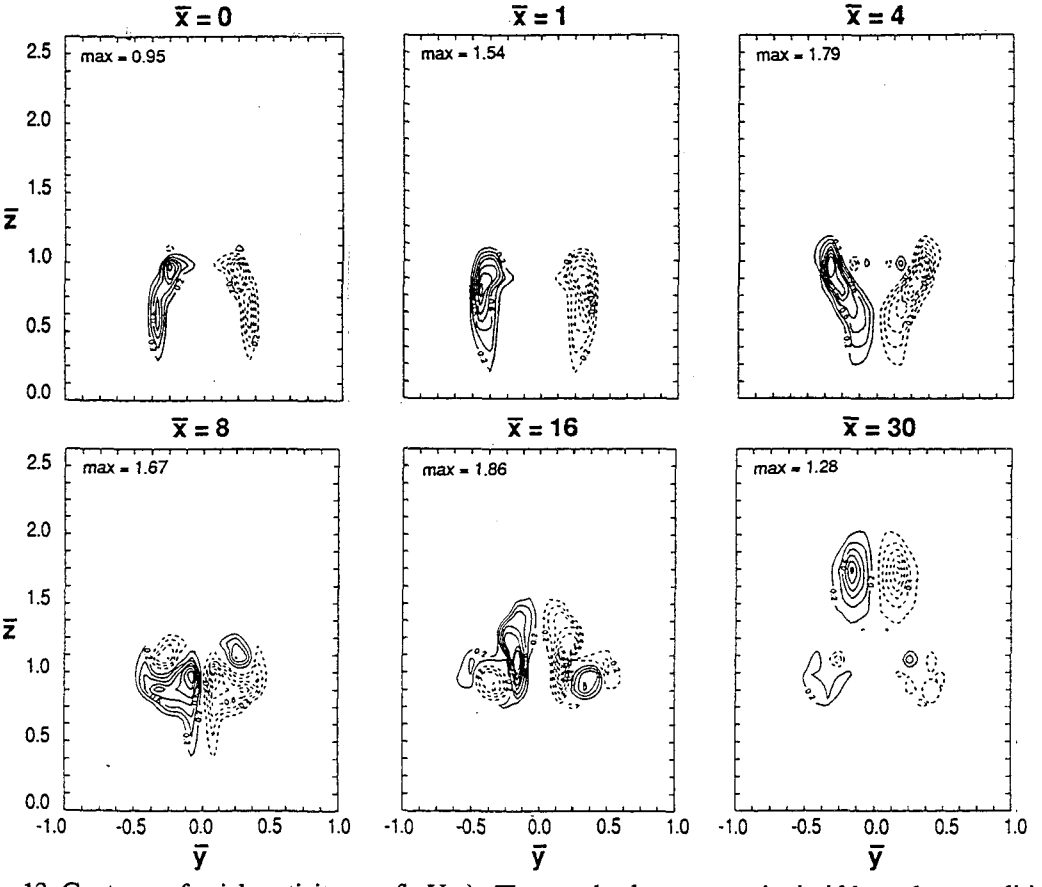

Figure 13. Contours of axial vorticity, $\omega_{\bar{x}}$ (h_j/U_∞). The no-shock geometry, inviscid boundary conditions.

interface as a result of baroclinic torque. The location of this vorticity at the base of the jet was responsible for the rapid and complete lift-off of the jet from the surface. Also note the cross-stream shear along the injectant/air interface in the exit plane. The sense of vorticity associated with this mechanism was the same as that of the shock-interaction.

The pressure field for the no-shock geometry is shown in Figure 12. The bow-shock generated by compression of the upper ramp surface led to high pressure above the ramp. Migration of the fluid from this high pressure region to the lower pressure region between the injector ramps was fundamental in producing cross-stream shear at the helium/air interface in the injection plane. For the inviscid boundary condition case, the flow about the ramps is irrotational except for vorticity associated with shock curvature. Vorticity contours for the no-shock geometry are shown in Figure 13. The vorticity was located relatively much higher in the flow field compared to that for the shock-enhancement geometry. The vorticity first influenced the upper portion of the jet, with the helium being pulled away from the wall rather than lifted from it.

Inclusion of finite boundary layers in the simulations resulted in more complicated axial vorticity signatures. The signatures were much like those for the baseline geometry shown in Figure 4. Two main points were recognized. 1)Upstream of the injection plane, in the trough between the ramps, significant turning of boundary layer vorticity and further diffusive flux were associated with interaction of the boundary layer with the ramp bow-shock. This vorticity was remote from the mixing interface. Its presence is marked by the vorticity in regions near the wall in the $\bar{x} = 0$ plot of Figure 4. 2) Downstream of the injection plane, further turning of vortex lines associated with the boundary layer was apparent due to interaction of the boundary layer with the strong axial vorticity field. This is also displayed by the contours shown for the baseline geometry in Figure 4. In all three geometries, because of the motion of the jet away from the wall, this vorticity had minimal impact on injectant mixing.

Analysis

Circulation: Shock-enhancement geometry

Figure 14 shows the non-dimensional circulation, $\bar{\Gamma} = \Gamma/U_\infty h_i$, for the shock-enhancement geometry with a free-slip boundary condition. Upstream of $\bar{x} = 0$, no axial vorticity was present in the flow field. The strong increase in circulation immediately following interaction of the injectant with the freestream is a direct measure of the magnitude of the cross-stream shear. Since the helium was injected parallel to the downstream combustor wall, the circulation is related directly to the ramp angle or

$$\bar{\Gamma}_{y\text{-}z} = \sin(\alpha_e) = 0.083$$

which compares very well with the level displayed by the numerical simulation.

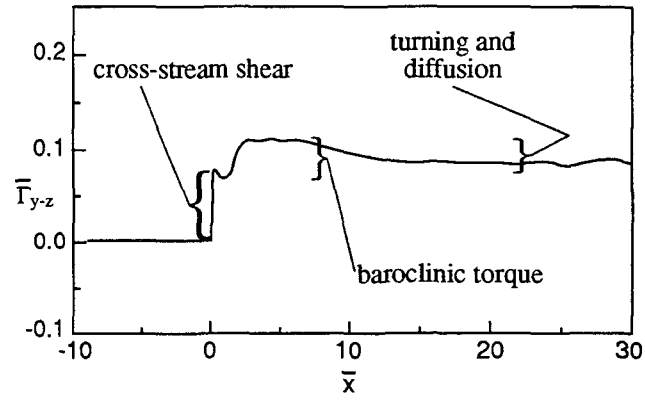

Figure 14. Circulation, shock-enhancement geometry, inviscid boundary conditions.

The additional circulation increase downstream of the injection point may be attributed to two sources: 1)shock interaction with the injectant/air density gradient , and 2)turning of the vorticity associated with the cross-stream shear. An estimate of circulation changes due to turning are presented following a discussion of the circulation associated with shock interaction.

A schematic of the complex shock interaction is shown in Figure 14. Shock waves propagate at different speeds in the different gases, expansion waves are present, reflections occur at the wall, and shock-shock interactions produce further vorticity. These complexities make analytical treatment of the circulation difficult.

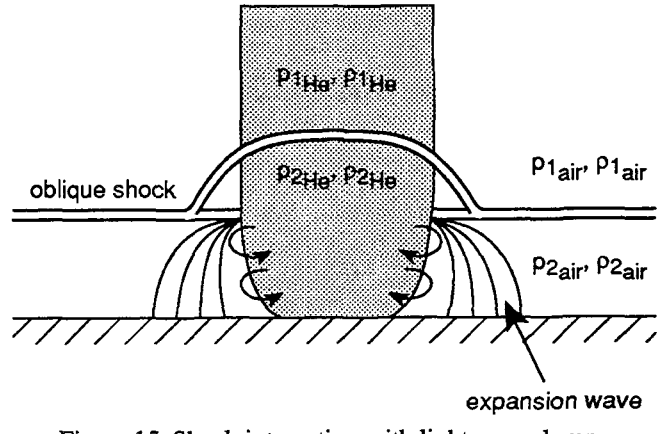

Figure 15. Shock interaction with light gas column.

Dimensional arguments, however, can be made to support a representation

$$\Gamma = \Delta\frac{1}{\rho}\Delta p\,\frac{L}{V_s}$$

for shock passage over a density interface, where L is the length of the interface, and V_s is the shock speed over the interface. The choice of expressions to represent the density and pressure change terms is not clear. With a simplified model as a guide, Yang[3] established approximations for these terms. He presented an expression for circulation that correlated data for the problem of Figure 2a within 15% over a broad range of Mach numbers and density ratios. Identical treatment to that of Yang is adopted here so that

$$\Gamma = \frac{\rho_{1He} - \rho_{1air}}{\frac{(\rho_{1He} + \rho_{1air})}{2}} \frac{(p_{2air} - p_{1air})}{\rho_{2air}} \frac{L}{V_s}$$

The thermodynamic quantities are subscripted to denote conditions prior to and after (1 and 2, respectively) shock passage. The expression is converted to the steady three-dimensional case by relating the shock speed to the freestream velocity

$$V_S = U_2 \tan(\beta - \alpha_e)$$

where β is the shock wave angle, α_e the change in wall angle, and U_2 the flow speed downstream of the shock. A $\cos(\beta - \alpha_e)$ term is required to represent the circulation associated with the axial component of vorticity. With these substitutions, the expression used to estimate the circulation attributed to shock-enhancement is

$$\bar{\Gamma}_{y\text{-}z} = \frac{\rho_{1He} - \rho_{1air}}{\frac{(\rho_{1He} + \rho_{1air})}{2}} \frac{(p_{2air} - p_{1air})}{\rho_{2air}} \frac{L}{U_2 \tan(\beta - \alpha_e)} \frac{\cos(\beta - \alpha_e)}{U_\infty h_i}$$

The shock angle, β, and the thermodynamic quantities were evaluated using adiabatic compressible flow relations for specified injectant and freestream conditions, and ramp geometry. Account was taken of a 30% reduction in interface length due to compression of the jet. The increase in circulation due to shock-impingement suggested by this correlation

$$\Delta\bar{\Gamma}_{y\text{-}z} = 0.06$$

compares reasonably well with the increase displayed by the data of Figure 14. Given the simplified representations of the gradients of pressure and density in the correlation, it is suggested only as a rough means to estimate circulation due to baroclinic torque.

For the inviscid boundary condition, two other phenomena produced changes in circulation downstream of the injection plane: turning of vortex lines, and diffusion of vorticity across the symmetry plane at $\bar{y} = 0$. (Even with no diffusion, the circulation would not be expected to remain constant since it is taken about a contour in the y-z plane. Fixed in orientation in this manner, the contour does not correspond to a material line.) Material lines were tracked through the flow field to judge the magnitude of turning. No estimate was made of the impact of diffusion. For $\bar{x} < 8$ the turning of cross-stream vortex lines was less than 3°, and the changes in circulation seen in this region resulted primarily from shock-impingement. For $\bar{x} > 8$, turning of vortex lines was as large as 10° - 15°. Given the magnitude of circulation in the cross and streamwise planes, the variations in circulation shown in Figure 14 for $\bar{x} > 8$ are reasonable.

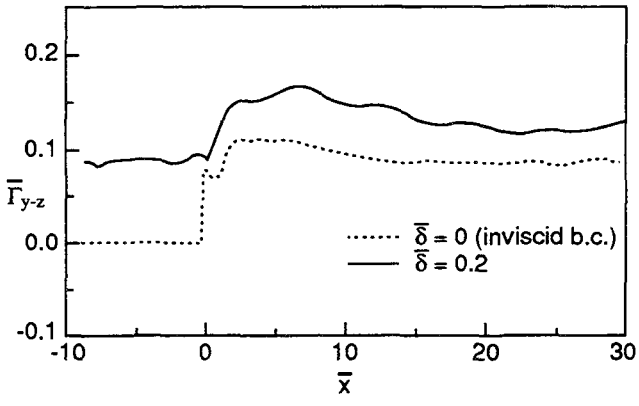

Figure 16. Circulation for the shock-enhancement geometry.

The effect of a finite boundary layer on the circulation for the shock-enhancement geometry is shown in the plot of Figure 16. Here, as expected, constant circulation associated with turned boundary layer vorticity is present upstream of the injection plane. It is this vorticity that produced cross-stream shear at the injectant interface after $\bar{x} = 0$. Finite boundary layers tended to obfuscate the presence of distinct vorticity sources downstream of the injection plane. This was due to the magnitude of circulation associated with the boundary layer. Turning of even five degrees produced significant variations in circulation in the cross-plane. For finite boundary layers, inclinations of nearly 90° were seen in some regions for vortex lines initially parallel to the y-axis. The turning was due to the proximity of strong streamwise vorticity associated with the jet that produced cross-stream pressure gradients along the combustor wall. Portions of the boundary layer were also entrained into the helium jet. This was particularly true for the $\bar{\delta} = 1.0$ case. The change in streamwise vorticity associated with this was not estimated.

Circulation: No-shock geometry

Circulation for the no-shock geometry for both viscous and inviscid boundary conditions is shown in Figure 18. As with the shock-enhancement geometry, the inviscid condition yielded much more readily to estimation of vorticity sources. For this case, the flow prior to $\bar{x} = 0$ should be irrotational except for vorticity from shock curvature. Consideration of Figure 5c shows that the majority of the vorticity produced from shock curvature for these geometries is not oriented in the axial direction. Also, estimates of the magnitude of the vorticity present

downstream of the ramp bow-shock were made using the expression[19]

$$\omega = -\frac{U_\infty}{r}\frac{\left(1 - \rho_1/\rho_2\right)^2}{\rho_1/\rho_2}\cos(\beta)$$

The estimates support the conclusion that shock curvature is not an important source of axial vorticity. Thus, the increase before $\bar{x} = 0$ must unfortunately be assigned to numerical errors along the boundary (particularly those associated with a rough grid edge[7] which produced strong localized entropy gradients in the flow field). The circulation after $\bar{x} = 0$ is associated with cross-stream shear at the exit plane.

Circulation for the no-shock geometry with viscous boundary conditions is also shown in Figure 17. The rise in circulation in the ramp region ($-6 < \bar{x} < 0$) was caused by secondary flow driven by pressure gradients. The increase was damped somewhat in the region $-3 < \bar{x} < 0$ due to axial vorticity of an opposite sense produced upon interaction of the ramp shock with the boundary layer in the channel between the ramps.

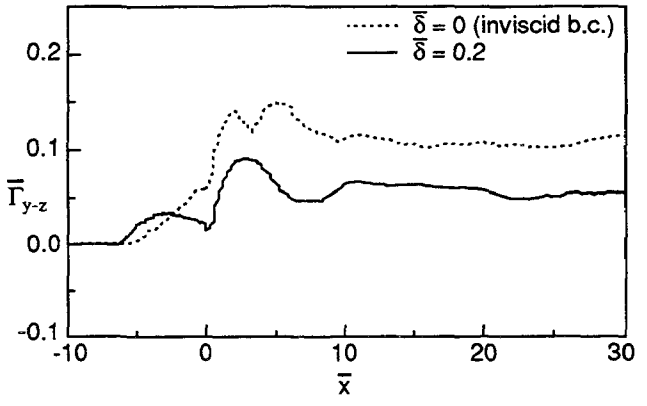

Figure 17. Circulation for the no-shock geometry.

Circulation: Baseline geometry

The final circulation plot, shown in Figure 18, is for the baseline geometry with a finite boundary layer.

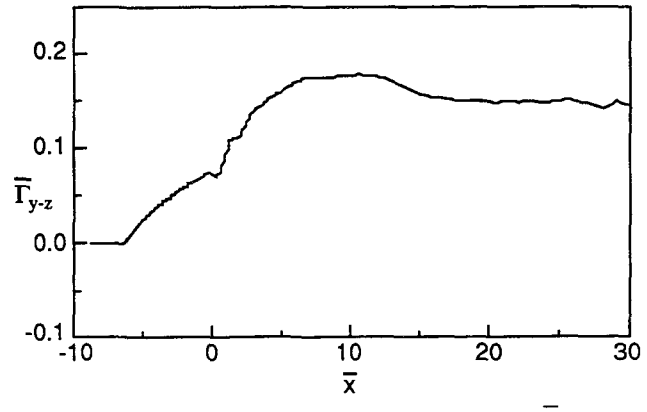

Figure 18. Circulation for the baseline geometry, $\bar{\delta} = 0.2$.

Recall that the shock-enhancement and no-shock geometries were designed so that the levels of circulation from baroclinic torque and cross-stream shear, respectively, were approximately the same as would be present for the composite baseline geometry. Elementary decomposition of the circulation shown in Figure 18 is limited by the unclear influence of the boundary layer. Interrogations of the numerical data set do support the presence of both mechanisms in the flowfield. Certainly, the larger magnitude of circulation for the baseline geometry may be indicative of the additive effects of both shock-enhancement and cross-stream shear.

Mixing

The ability of streamwise vorticity to mix the injectant with the freestream is influenced by magnitude, scale and proximity to the mixing interface. The previous section was devoted to characterizing the different axial vorticity sources in terms of their impact on circulation. The measure can often be misleading however, since it is an integral measure, and for instance takes no account of the location of the vorticity in the flow field. (Considering location is particularly important for cases with finite boundary layers where strong vorticity is present remote from the mixing interface.)

Mixing of the injectant with the freestream was treated only in the sense that it could be represented in the numerical simulation. This limited consideration to mixing driven by large-scale, time-mean, kinematical processes and diffusion. Further, the results are influenced by numerical dissipation and requisite spatial discretization. Support for the qualitative value of these results comes from the comparisons with experiments presented by Waitz, Marble and Zukoski.[8,9]

The numerical results allowed for detailing the percent of total helium mass flux present in each concentration band as mixing evolved downstream of the injection plane. Plots of

$$\frac{\dot{m}_{He}}{\dot{m}_{He\text{-}total}} \quad vs. \quad c_{He} \quad vs. \quad \bar{x}$$

are presented to characterize the mixing. From these plots, three measures of the efficacy of the mixing process were noted: 1) The point downstream of injection where there was no longer any pure injectant in the plane, i.e. 0% $\dot{m}_{He}$ at $c_{He} = 1.0$, 2) The rate of decay of $c_{He\text{-}max}$ in $\bar{x}$, and 3) the percentage of the total helium mass flux occurring at $c_{He} \leq 0.05$, as a function of $\bar{x}$.

Plots of this data are shown in Figure 19 for the three-geometries investigated with $\bar{\delta} = 0.2$. Comparison between the two plots for the shock-enhancement geometry and the no-shock geometry (Figures 19 a. and b.) shows that pure helium no longer existed in the flow field by $\bar{x} = 15$ for the

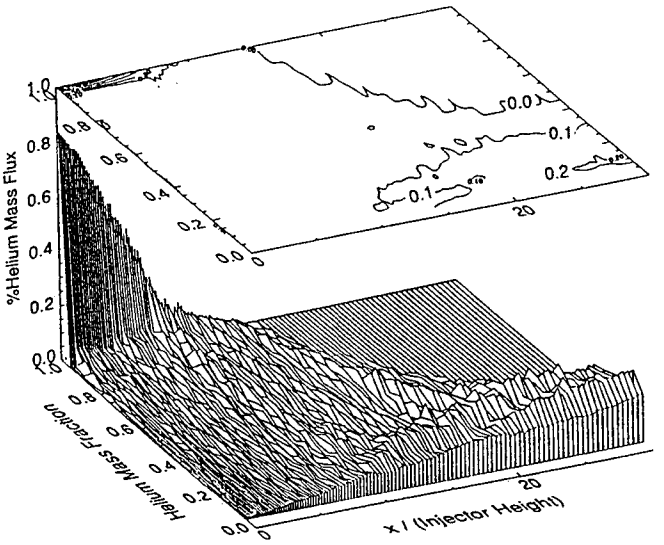

a. shock-enhancement geometry

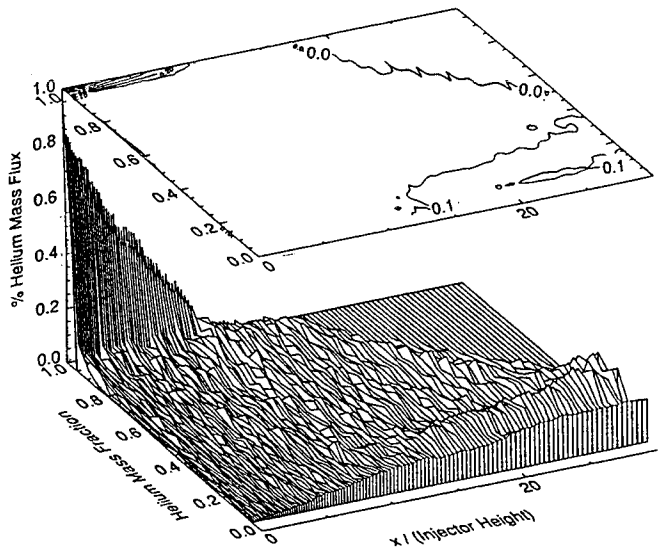

b. no-shock geometry

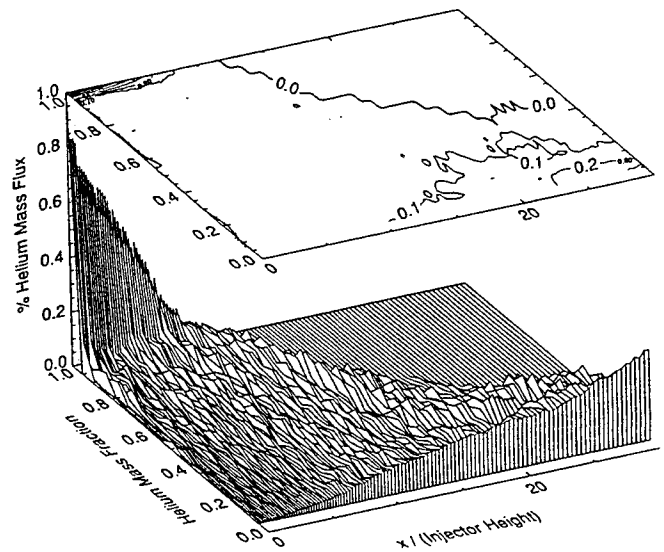

c. baseline geometry.

Figure 19. Mixedness measure data, $\bar{\delta} = 0.2$.

shock-enhancement geometry and $\bar{x} = 17.5$ for the no-shock geometry. The decay of maximum helium concentration is more rapid for the former also. The percent of total helium mass flux mixed to $c_{He} \leq 0.05$ (this is denoted by the height of the lower edge of the carpet plot) was 18% for the shock-enhancement geometry and 16% for the no-shock case at $\bar{x} = 30$. While the differences are not large, they are significant and typical of those for the $\bar{\delta} = 0.0$ (free-slip b.c.) and $\bar{\delta} = 1.0$ cases as well.

Comparing the data for the baseline geometry (Figure 19c) with that for the other two geometries supports the additive nature of the primary vorticity sources. For this case, there was no longer any pure helium by $\bar{x} = 12$, and 35% of the helium mass flux was mixed below $c_{He} = 0.05$ by $\bar{x} = 30$.

The reasons for the better performance of the geometries employing shock-enhancement are likely two-fold: 1) the magnitude of streamwise circulation, and 2) location of vorticity with respect to the fuel/air interface. While qualitatively, the first of these should be considered the most important, the difference in location of the primary vorticity sources can not be discounted. Shock-impingement provides for deposition of vorticity precisely where it is desired: on the light/heavy gas interface. The vorticity associated with cross-stream shear is displaced from the mixing interface. This point is possibly made clearer through consideration of the diagrams of Figure 20. Analogous two-dimensional shear layer models appear above the cases for both cross-stream shear and baroclinic torque. Displacement of the interface from the location of the vorticity will impact both large-scale convection of the interface, and shear mixing along the interface.

Conclusions

Previous experimental and numerical studies of a class of contoured wall fuel injectors aimed at enabling shock-enhanced mixing were unable to resolve the relative importance of various axial vorticity sources in mixing the injectant with the freestream. This study has shown that two important sources exist. The first is associated with baroclinic torque due to shock-impingement on the injectant/air density interface. The second is cross-stream shear driven by pressure gradients associated with the ramp geometry. Geometries employing shock-enhancement were found to be most effective in mixing the injectant with the freestream. This was attributed to larger magnitude streamwise circulation and the fact that vorticity was deposited directly on the helium/air interface. The vorticity associated with cross-stream shear was displaced a short distance from the fuel/air interface. Turning of vortex lines associated with the boundary layer produced axial vorticity of magnitude and extent that affected levels of circulation, but since the vorticity was largely remote from the mixing interface, the impact on mixing was negligible. Levels of axial vorticity associated with shock curvature upstream of the injection point were also found to be negligible.

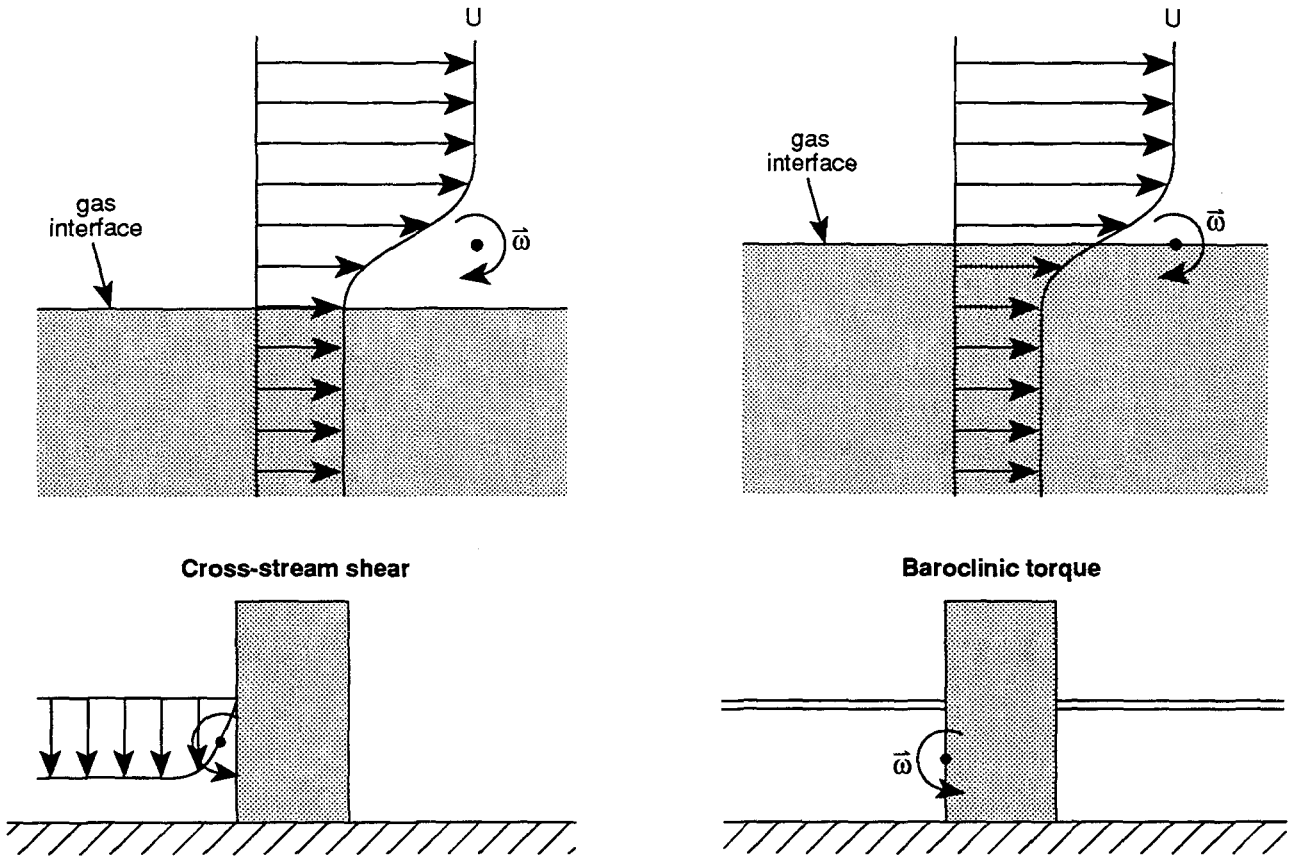

Figure 20. Location of primary axial vorticity sources with respect to the mixing interface, and analogous two-dimensional shear flows.

Acknowledgments

Funding for this work was provided largely through NASA Grant NAG 1-842. The fundamentals of shock-enhanced mixing were developed earlier under Contract F49620-86-C-0113 administered by the Air Force Office of Scientific Research. The authors wish to thank many members of the technical staff at NASA Langley Research Center, particularly D. Bushnell, S. Robinson, M. Walsh, members of the Experimental Flow Physics Branch, and members of the Computational Methods Branch. Supercomputing support was provided by the San Diego Supercomputer Center via a National Science Foundation Grant, the NASA Ames NAS facilities, the JPL/Caltech Cray, and the NASA Langley supercomputing facilities.

References

1. Manning, T. A., "Experimental Studies of Mixing Flows with Streamwise Vorticity," S. M. Thesis, Massachusetts Institute of Technology, Cambridge, Massachusetts, September 1991.

2. Marble, F. E., Hendricks, G. J., and Zukoski, E. E., "Progress Toward Shock Enhancement of Supersonic Combustion Processes," AIAA Paper 87-1880, 1987.

3. Yang, J., "An Analytical and Computational Investigation of Shock-Induced Vortical Flows with Applications to Supersonic Combustion," AIAA Paper 92-0316, 1992.

4. Drummond, J. P., "Mixing Enhancement of Reacting Parallel Fuel Jets in a Supersonic Combustor," AIAA Paper 91-1914.

5. Haas, F., and Sturtevant, B., "Interaction of Weak Shock Waves with Cylindrical and Spherical Gas Inhomogeneities," J. Fluid Mechanics, v. 181, pp. 41-76, 1987.

6. Marble, F. E., Zukoski, E. E., Jacobs, J. W., Hendricks, G. J., and Waitz, I. A., "Shock Enhancement and Control of Hypersonic Mixing and Combustion," AIAA Paper 90-1981, 1990.

7. Waitz, I. A., "An Investigation of Contoured Wall Injectors for Hypervelocity Mixing Augmentation," Ph. D. Thesis, California Institute of Technology, Pasadena, California, 1991.

8. Waitz, I. A., Marble, F. E., and Zukoski, E. E., "An Investigation of a Contoured Wall Injector for Hypervelocity Mixing Augmentation," AIAA Paper 91-2265, 1991.

9. Waitz, I. A., Marble, F. E., and Zukoski, E. E., "A Systematic Experimental and Computational Investigation of a Class of Contoured Wall Fuel Injectors," AIAA Paper 92-0625, 1992.

10. Carpenter, M. H., "Three-Dimensional Computations of Cross-Flow Injection and Combustion in a Supersonic Flow," AIAA Paper 89-1870, 1989.

11. Eklund, D. R., Northam, G. B., and Fletcher, D. G., "A Validation Study of the SPARK Navier-Stokes Code for Nonreacting Scramjet Combustor Flowfields," AIAA Paper 90-2360, 1990.

12. Northam, G. B., Greenberg, I., and Byington, C. S., "Evaluation of Parallel Injector Configurations for Supersonic Combustion," AIAA Paper 89-2525, 1989.

13. Drummond, J. P., Carpenter, M. H., Riggins, D. W., and Adams, M. S., "Mixing Enhancement in a Supersonic Combustor," AIAA Paper 89-2794, 1989.

14. Riggins, D. W., Mekkes, G. L., McClinton, C. R., and Drummond, J. P., "A Numerical Study of Mixing Enhancement in a Supersonic Combustor," AIAA Paper 90-0203, 1990.

15. Riggins, D. W., and McClinton, C. R., "A Computational Investigation of Flow Losses in a Supersonic Combustor," AIAA Paper 90-2093, 1990.

16. Riggins, D. W., and McClinton, C. R., "Analysis of Losses in Supersonic Mixing and Reacting Flows," AIAA Paper 91-2266, 1991.

17. Riggins, D. W., and McClinton, C. R., "A Computational Investigation of Mixing and Reacting Flows in Supersonic Combustors," AIAA Paper 92-0626, 1992.

18. McCormick, D. C., "Vortical and Turbulent Structure of Planar and Lobed Mixer Free-Shear Flows," Ph. D. Thesis, The University of Connecticut, 1992.

19. Hayes, W. D., and Probstein, R. F., Hypersonic Flow Theory, Academic Press, New York, 1959.